X-57 Ground Dynamics Modeling and Analysis

Loren J. Newton[1] and Ryan D. Wallace[2]
NASA Armstrong Flight Research Center, Edwards, California, 93525, U.S.A.

This paper presents simulation work to assess the ground handling behavior of the X-57 airplane, prior to its first flight under electric propulsion. A tire deformation model was fit to manufacturer ground testing data to develop a detailed simulation model of previously unmodeled rolling drag forces on the tires. A special modeling effort corrected for a difference between the runway surface in the manufacturer data (grass) and in intended X-57 surface operations (asphalt/concrete). Analysis based on variation in the test conditions of the manufacturer test data showed that uncertainty in the new estimated rolling drag model should lead to no more than 1.5-percent uncertainty in the takeoff acceleration. Another batch simulation series swept across ground operating conditions and airplane configurations, characterizing turning radii and roll angles experienced for different open-loop steering commands in these various situations. This simulation allowed the identification of ground handling characteristics even beyond the regime of normal operations. As part of this task, a new, modified variant of the Fibonacci search algorithm identified the correct steering inputs for maintaining a straight path as a function of the operating condition. Finally, this paper describes a fixed-base piloted simulator assessment. This assessment supplements the previous simulated ground dynamics data with pilot-in-the-loop data and pilot feedback and confirms the overall acceptability of the ground handling qualities of the X-57 airplane prior to first flight.

I. Nomenclature

b	=	tire width
D	=	longitudinal (drag) force
F	=	normal force
f	=	final state
h	=	soil height
i	=	ideal full-compression state
k	=	rolling resistance coefficient
R	=	turning radius
r	=	wheel radius
u	=	soil compressibility integration parameter
V	=	ground speed
α	=	perturbation hyperparameter
β	=	drifting hyperparameter
γ	=	scaling hyperparameter
ρ	=	soil density
μ	=	rolling friction coefficient
λ	=	soil void ratio
σ	=	soil compressive strength
ϕ	=	slip ratio
Ω	=	wheel angular velocity

[1] Engineering Student Trainee, Dynamics and Control Branch, AIAA Member.
[2] Aeronautical Engineer, Dynamics and Control Branch, AIAA Member.

II. Introduction and Background

The X-57 "Maxwell" airplane is a distributed electric propulsion flight demonstrator developed by the National Aeronautics and Space Administration (NASA). The airplane is the first all-electric experimental piloted airplane belonging to the agency. Possible benefits of distributed electric propulsion include greater high-speed cruise efficiency, reduced noise compared to traditional internal combustion engines, and the elimination of in-flight carbon emissions. Through the X-57 program NASA seeks to develop certification standards for the design and operation of electric aircraft and share with industry technical lessons and best practices from the process of taking the aircraft to flight [1].

The X-57 airframe itself is derived from the Tecnam® P2006T (Costruzioni Aeronautiche Tecnam) (Capua, Italy) twin-piston engine, general aviation airplane. The project is organized in the form of four phases. The first phase, or modification ("Mod") I, used a stock P2006T airplane that was flown to assess baseline performance qualities. Mod II is the first phase with electric propulsion introduced; the two internal combustion engines of the factory P2006T airplane are replaced at their original stations with two 60-kW electric cruise motors. In Mod III, the P2006T wing will be replaced by a higher aspect ratio wing. The cruise motors will also be relocated to the wingtips with the intention of reducing the wingtip vortex drag. In the final configuration, Mod IV, twelve high-lift 10.5-kW electric motors will be installed along the length of the wing. This distributed propulsive system will be activated during takeoff and landing to recover lift and allow the X-57 airplane to attain performance during critical phases of flight, similar to the factory P2006T airplane. During cruise flight, the high-lift motors will shut off, and the propellers will fold back along the nacelles to reduce drag. Mods II through IV are illustrated in Fig. 1.

a) Mod II.

b) Mod III.

c) Mod IV.

Fig. 1 Illustrations of X-57 modifications with electric propulsion.

To predict the dynamics of each of the Mods and to train for flight-testing, an X-57 simulation has been developed that is capable of batch and piloted simulations. The simulations of Mods I and II were used to perform all of the work in this paper. The aerodynamic models for these Mods are based primarily on parameter identification analyses from

instrumented test flights of a P2006T airplane. The electric propulsion model consists of a proportional torque motor command and a constant speed propeller system derived from a blade element analysis in the commercial off-the-shelf XROTOR (open-source software, Massachusetts Institute of Technology) (Cambridge, Massachusetts) software package. The X-57 landing gear model architecture was adapted from legacy NASA simulation software. The legacy NASA model provided a generic architecture that included the critical landing gear properties of nosewheel steering (NWS), tire traction, strut dynamics, and wheel braking. Airplane landing gear specifications from Tecnam® and the tire manufacturer, with estimated tire and strut properties from the initial instrumented P2006T flights, were then input into the landing gear model architecture to make the model X-57 specific. Vertical gear forces were calculated based on the strut displacements of nose gear and main gear. The horizontal longitudinal and lateral forces were determined from ground-tire interaction constants and vertical loads. The X-57 subsystem models were then integrated into the Langley Research Center (LaRC) (Hampton, Virginia) desktop simulation, developed in MATLAB Simulink (The MathWorks, Inc.) (Natick, Massachusetts) software, and were used for batch simulation studies and further model development. The LaRC simulation is integrated into the fixed-base Armstrong Flight Research Center (AFRC) (Edwards, California) piloted simulator at NASA AFRC, which is used for pilot evaluation and training in addition to batch analyses.

This paper describes work to model the behavior of the X-57 Mod I and II on the ground during taxi, takeoff, and landing operations. A more detailed model of the P2006T landing gear dynamics, including velocity-dependent rolling resistance terms was developed and integrated into the simulation. Since ground dynamics are driven by a combination of aerodynamic effects and tire forces, updating the landing gear model with these terms that model more realistic phenomena such as tire deformation allows tire drag forces to be modeled more accurately, improving the understanding of how the airplane may react in ground handling maneuvers. Simulator tests featuring this updated model, including both batch analyses and piloted handling qualities evaluations, were then conducted to capture more precisely the ground handling characteristics of the X-57 airplane, such as roll angles in a turn, turning radius, and piloted handling qualities, prior to ground and flight-testing in the actual airplane.

III. Rolling Friction and Resistance

A. Modeling

To improve the landing gear model, a more detailed model of the drag forces on the rolling wheels was integrated in the simulation. This new model accounts for not only friction like the legacy model but also rolling resistance, or tire deformation as a function of velocity and material properties. Capturing the longitudinal forces on the tire accurately is important to properly assess the ground handling qualities of the X-57 airplane, which will be analyzed in later sections. Flight data were used to fit the new model that captures these contributions to the longitudinal tire force. During the initial flight-testing of the P2006T airplane, Tecnam® recorded several velocity time histories during takeoff rolls [2]. This data serves as a reference for the simulated landing gear dynamics, as the X-57 airplane utilizes the stock P2006T landing gear, and in particular the Mod I simulation shares the same mass properties as the stock P2006T airplane. The only difference between the stock P2006T airplane and the Mod I simulation is that the simulation uses electric motor models for propulsion. These models, however, are adjusted to closely match the thrust performance of the P2006T piston engines. The simulated Mod I takeoff velocity profile should thus closely match the Tecnam® data, given similar takeoff configurations, input commands, and runway environments. The parameters of the new rolling drag model could be tuned in the simulation until this agreement is realized. Unfortunately, the published Tecnam® data were collected on a grass airfield. Meanwhile, the X-57 airplane will operate exclusively from paved asphalt or concrete runways. To properly apply the Tecnam® data for model fitting, it was thus critical to identify different characteristics of these surfaces and how they would impact the resulting rolling drag.

Longitudinal rolling drag can be decomposed into several components: rolling friction drag D_{RF} and two rolling resistance drag terms $D_{RR,TD}$ and $D_{RR,C}$, as shown in Eq. (1). These components will be described in detail below.

$$D_{total} = D_{RF} + D_{RR,TD} + D_{RR,C} \tag{1}$$

Rolling friction is a drag force resulting from the horizontal tractive shearing experienced at the contact patch between the tire and the ground surface. It is equal to the normal force scaled by the rolling friction coefficient μ. Generally, μ is a nonlinear function of slip ratio ϕ [3]. Slip ratio is given as a function of wheel angular velocity Ω, wheel radius r, and airplane ground speed V, as shown in Eq. (2):

$$\phi = \frac{\Omega r}{V} - 1 \tag{2}$$

On the P2006T/X-57 landing gear, however, the wheels are not driven, meaning that no driving torque is directly applied to the wheel shafts. Moreover, the Tecnam® test data were recorded during a takeoff roll; thus, no torque from pilot-applied braking was present in the data. In the absence of driving or braking torques (assuming zero wheel-bearing friction), $\Omega r = V$ and a no-slip scenario is realized. The objective of the data-driven analysis in estimating rolling friction can then be reduced to estimating a single friction coefficient μ_{max} (rather than a function $\mu(\phi)$). Equation (3) shows the rolling friction drag D_{RF} is then simply:

$$D_{RF} = \mu_{max} F_Z \tag{3}$$

Meanwhile, when the airplane is in contact with the ground, work is done deforming both the tire and the ground surface. Rolling resistance captures drag that results from this deforming work [4]. The rolling resistance drag due to tire deformation $D_{RR,TD}$ is independent of the particular surface the tire is rolling on and is instead only a function of the translational velocity V of the wheel and the normal force F_Z experienced by the wheel [5]. This function is given in Eq. (4) [5], where V has units of km/h. The empirical coefficients of this equation k are functions of the material properties of the tire itself.

$$D_{RR,TD} = \left(k_{R1} \left(\frac{V}{100} \right) + k_{R4} \left(\frac{V}{100} \right)^4 \right) F_Z \tag{4}$$

Rolling resistance drag because of vertical compression of the ground $D_{RR,C}$, on the other hand, innately depends on the material properties of the ground per Eqs. (5-6) [6] and is more critical for soft, unpaved surfaces. For materials such as asphalt or concrete, the vertical compression of the ground is negligible because of the relatively high compressive strengths of the materials [3].

$$D_{RR,C} = \frac{b \sigma_i \rho_0 h_0}{\rho_i \sqrt{\lambda}} \int_{u_f}^{u_0} e^{-u^2} du \tag{5}$$

where

$$u = \sqrt{\lambda} \left(\frac{\rho}{\rho_0} - 1 \right) \tag{6}$$

The subscript 0 represents the initial state prior to compression, *f* represents the final state under the compression of the tire, and *i* represents a theoretical state where the soil is as compressed as physically possible. The soil parameters σ, λ, and ρ represent compressive strength, void ratio, and density, respectively; h represents the thickness of the soil layer, and b is the mean width of the tire.

A final type of rolling drag on the tire is from horizontal ground deformation: the tire pushing material out of the way to the sides as it rolls [6]. This penalty is typically reserved for loose soils or long grass, where the wheel will need to clear its own path in order to move forward. Again, for paved surfaces this drag is negligible since there will be no loose material for the wheel to displace. Moreover, even for well-maintained grass runway strips this drag may still be ignored as there will not be a significant amount of vegetation impacting the wheel.

With these assumptions in place, the Tecnam® published data could be used to tune the landing gear rolling drag model by fitting the coefficient μ_{max} of Eq. (3) and the coefficients k_{R1} and k_{R4} of Eq. (4). First, the total rolling drag could be modeled for grass runway operations based on the Tecnam® velocity data. In order to represent a paved surface, the constant vertical compression drag could then be subtracted from the resistance, and the rolling friction could be corrected to an asphalt value based on literature. Note that the horizontal deformation drag is assumed to be negligible throughout the scope of this process, as only a well-maintained grass runway strip (Tecnam® data) and paved runways (intended use) are being considered.

The drag due to vertical compression of the grass runway can be calculated using geological data. The Capua region of Italy, where Tecnam® conducted its flight-tests, is characterized by xeric, volcanic soil with a relatively high-moisture content in the winter, when the takeoff data were recorded [7]. Selecting representative soil parameters [8-9] and substituting into Eq. (5) gives drag forces of no more than approximately 1.0 lbf (4.6 N) for the nose wheel, and 1.2 lbf (5.5 N) for each main wheel. This vertical compression drag is typically motivated by analyses of snowy surfaces [6], where much more compression is observed. On a grass runway, however, this drag has a nearly negligible impact on the rolling resistance but can be easily included in the analysis anyways.

Next, the coefficients k_{R1} and k_{R4} of Eq. (4) must be estimated. The Tecnam® data included several complete takeoff roll velocity profiles that were sampled at a rate of one sample per second. These time histories were synchronized and averaged together to produce a single velocity profile reference. Meanwhile, the desktop simulation was configured to simulate a takeoff roll: a straight-line acceleration from a resting state. Per the operating handbook

for the P2006T airplane, the takeoff flap position of 20-degree of flaps was commanded, and the elevator was held neutral during acceleration up to 55- kn indicated airspeed (IAS) [2]. The portion of the simulator velocity data in this regime, from initial movement to 55-kn IAS, was compared to the published takeoff roll data. The published data were interpolated to match the sample rate of the simulator; the mean-squared error (MSE) between these two signals served as the error metric for the function-fitting task.

Essentially, the rolling drag estimation task seeks to make the two signals match by adjusting three parameters in the simulation. These parameters comprise of the material-dependent surface friction coefficient and the coefficients in the quartic velocity-dependent tire deformation drag equation, Eq. (4): a feature vector of $[\mu_{max}, k_{R1}, k_{R4}]$. To reduce the number of simulations that were run, a gradient-free algorithm, the Hooke-Jeeves pattern search, was used to select these coefficients [10]. In each iteration of the Hooke-Jeeves method, six simulations were run: in each simulation, one of the three parameters was perturbed from its current estimate by $\pm\alpha$. The algorithm calculates the mean-squared error (MSE) between the simulation velocity profile and the published data truth source for each perturbation and saves the perturbation that most reduces the MSE compared to the previous iteration. If no MSE improvements are found, α is reduced in size by a scaling factor γ. The method converges when α reaches a threshold small value.

In the Hooke-Jeeves implementation used here, a scaling factor of $\gamma = 0.5$ and an initial perturbation value of $\alpha = 0.1$ was used with the search terminating when α reached 5×10^{-4}. The feature vector was initialized to $[0.35, 0.1, 0.1]$. The search concluded on values of $\mu_{max} = 0.3875$, $k_{R1} = 0.102$, and $k_{R4} = 7.03 \times 10^{-4}$. The surface friction coefficient is in the ballpark of expected values for a rubber tire rolling on grass, between 0.3 and 0.4. To check the values of these parameter estimates, the fit rolling resistance function and updated friction coefficient were integrated into the landing gear model in the LaRC desktop simulation. A simulated takeoff roll replicating those from the Tecnam® test program was simulated. Figure 2 illustrates the absolute (top) and percent (bottom) error between the simulated velocity time history and the Tecnam® measured flight data, plotted as a function of the velocity during the takeoff roll.

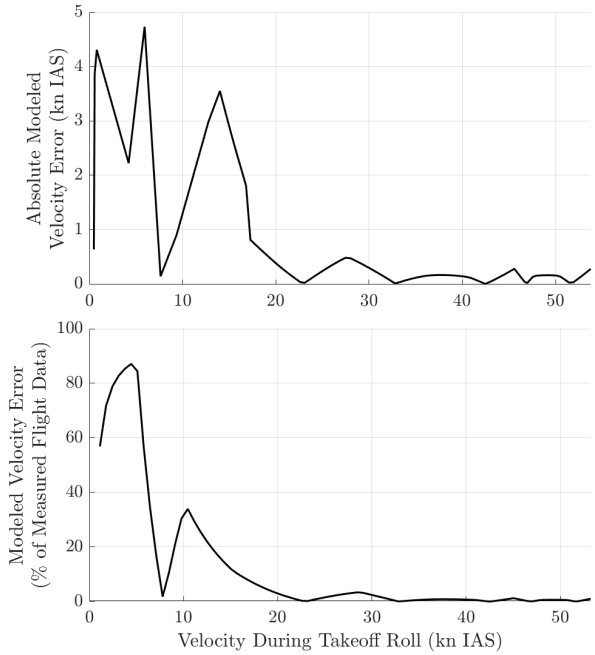

Fig. 2 Comparison of the model velocity profile, and the measured velocity profile during a takeoff roll.

The biggest disagreements between the simulator and the Tecnam® data occurred at the beginning of the takeoff roll, at speeds below 20-kn IAS; however, this disagreement was not deemed to be noteworthy: the recorded Tecnam® data came from a pitot tube, which bears less responsive readings at low airspeeds. It is noteworthy, however, that all Tecnam® datasets used in this analysis had identical behavior at or below 15-kn IAS but featured significant variation between different trials at higher speeds. This result suggests that the velocity data recorded at very low speeds may not be of any merit because of the air data measurement limitations. The discrepancy between the simulation and the

Tecnam® data at low speeds is thus not perceived to be of any concern; otherwise, the simulated velocity profile on the takeoff roll agrees very well with the Tecnam® data.

With the grass runway takeoff roll modeled, the vertical compression drag was disabled in the simulation, and the rolling friction was changed to 0.72 to capture tire dynamics on an asphalt runway [11]. The velocity-dependent tire deformation drag function remained the same. Modeling the velocity-dependent term and incorporating it into the simulation caused the airplane to require 2.2 additional seconds to reach its rotation speed on takeoff. For a takeoff roll that requires less than 20 seconds to achieve rotation speed, this time duration is a significant change that was previously unmodeled.

B. Uncertainty Analysis

A simple uncertainty analysis was performed to see how uncertainty and error in the prescribed Tecnam® test conditions may propagate to the estimated resistance and friction parameters. This analysis gives intuition as to the sensitivity of each parameter based on physical conditions. Moreover, insight is given into how much error may be inherent in the drag parameters as a result of reasonable errors in assumptions concerning the physical test conditions. Bounds on this "parameter uncertainty" could then be used to determine how much uncertainty there may be in the simulated airplane kinematics and resulting ground handling characteristics, specifically owing to the rolling resistance model.

Four physical test conditions were perturbed: simulated airplane weight, center of gravity location, total engine thrust, and vertical soil compression drag force. In the Tecnam® flight-test publication, the airplane was flown at maximum takeoff weight and full-forward center of gravity; however, the four flight profiles recorded were flown consecutively. Each of these resulting values would then be expected to have changed over the course of the approximately 30-minute flight, up to about 1-percent from their nominal values. While each takeoff roll was flown at full throttle, thrust was also assumed to vary up to about 1-percent from the maximum value. Finally, since the vertical compression drag was based on less concrete assumptions about the operating condition, it was perturbed by values on the order of 100 percent. Three perturbations were analyzed for each physical test condition.

Each physical test condition perturbation was individually implemented in the desktop simulation. The Hooke-Jeeves algorithm was once again applied, tuning the three drag parameters to fit the simulation readouts to the Tecnam® data under each perturbed flight condition. This data resulted in four points (three perturbations and the nominal test condition) for percent change in each estimated parameter as a function of percent perturbations in each physical condition. Figure 3 illustrates the information that was gathered in this process for an example pairing of a drag parameter and physical test condition.

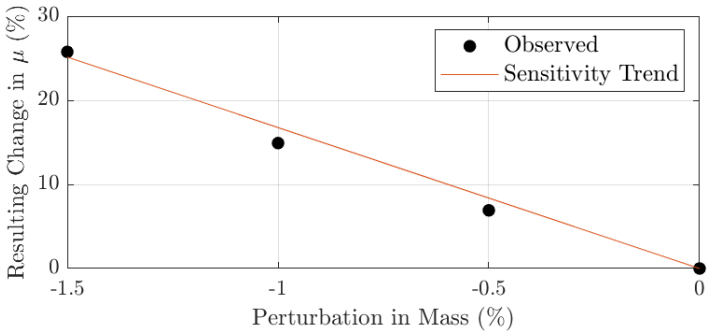

Fig. 3 Example of the sensitivity data: changes in the rolling friction estimate as a function of perturbations in the simulated airplane mass.

Since there are three parameters and four physical conditions, this leads to twelve total functions. The slope of the best-fit line for each function indicates the sensitivity of a particular parameter to a perturbation in a particular physical test condition, or what percentage change of a parameter value is expected for a 1-percent change in the test condition. Table 1 collects the calculated sensitivity of each parameter to each test condition.

Table 1 Estimated parameter sensitivities: changes in response to a 1-percent perturbation in each test condition.

Estimated parameter	Test condition			
	Mass	Center of gravity	Thrust and aerodynamic drag	Compression drag
μ_{max}	-16.8%	-6.99%	-20.1%	0.296%
k_{R1}	-6.70%	-0.67%	-2.09%	0%
k_{R4}	31.5%	16.8%	57.1%	-0.0133%

This data has several interesting features. First, all three parameter sensitivities with respect to the vertical compression drag were less than one percent, which makes intuitive sense given how small the drag forces were compared to friction and rolling resistance.

On the other hand, k_{R4} was notably sensitive to the three test conditions other than the vertical compression drag. This, however, is both somewhat expected and not critical to the takeoff roll analysis. The quartic term in Eq. (4) is generally small for velocities below 100 km/h (54 knots (kn)), which is nearly the entire envelope for the takeoff roll since the rotation speed of the P2006T airplane is specified as 64 knots. The quartic term would then both be expected to be exceptionally small for most of the Tecnam® data, making k_{R4} difficult to estimate with much certainty. At the same time, since that term is so small, this variation in k_{R4} would not impact the deformation drag for much of the takeoff roll anyway.

The other parameter that had estimation sensitivities above 10 percent was μ_{max}, which was very sensitive to the simulated airplane weight and thrust. The nominal estimated value of μ_{max}, however, agreed with the expected value of a rubber tire rolling on grass; the value was thus accepted with the understanding that it was simply sensitive to the test conditions, and not inherently an uncertain estimate.

This analysis characterized the plausible variability of the estimated parameters with regards to plausible variations in the test conditions. This variability was then used to define a range in which each of the true values of the parameters were expected to lie, constrained by the reasonable range of flight conditions in the fitting data. The bounds for each expected parameter value are driven by the approximate expected perturbation in the physical test conditions (100 percent for vertical compression drag, one percent for the other three conditions), multiplied by the corresponding sensitivities; the entries of each row are shown in Table 1. In the simulation, different values of each parameter were tested to see how uncertainty in the estimated model parameters may propagate to the physical quantity of concern: the takeoff velocity profile. More specifically, the takeoff "acceleration time," from full throttle command to rotation speed, was recorded for each parameter configuration.

To fully capture the overall behavior of perturbations to the parameters, parameter values were also tested outside of the plausible range. Figure 4 shows how the acceleration time varied as a function of the rolling drag parameters moving away from their nominal estimated values. A generally linear relationship was found, particularly within the expected plausible range.

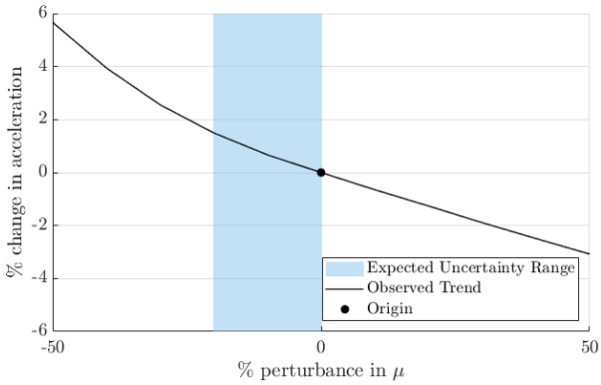

a) **Sensitivity to μ_{max}.**

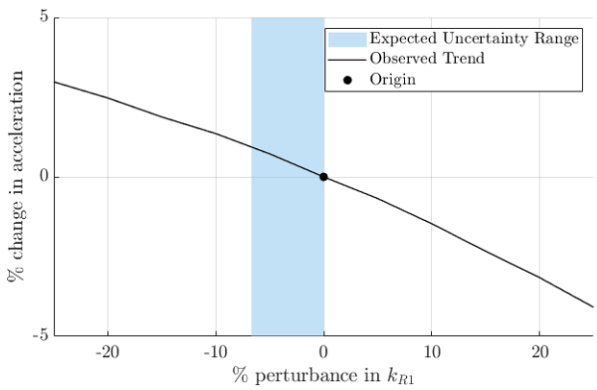

b) **Sensitivity to k_{R1}.**

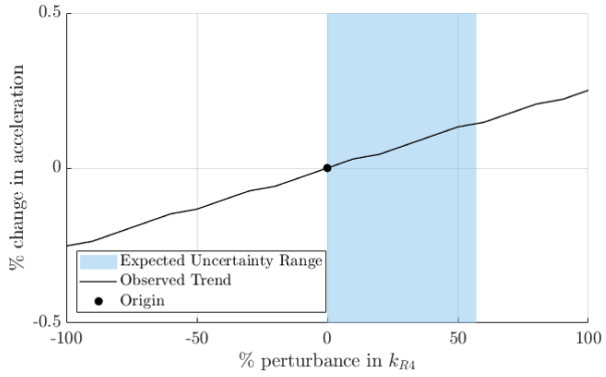

c) **Sensitivity to k_{R4}.**

Fig. 4 Change in acceleration time as a result of variation in each of the estimated parameters.

Table 2 quantitatively summarizes the key conclusions from Fig. 4, that is: how much uncertainty exists in the acceleration time within the plausible regime of estimated parameter variation. This effectively summarizes how bounded uncertainty in the physical test condition propagates to uncertainty in the physical velocity measurement.

Table 2 Acceleration uncertainty because of expected uncertainty in the estimated parameters.

Estimated parameter	Physical condition of greatest sensitivity	Expected bounds of parameter uncertainty	Expected bounds of acceleration uncertainty
μ_{max}	Thrust	[-20.1%, +0%]	[-1.26%, +0%]
k_{R1}	Mass	[-6.7%, +0%]	[-0.946%, +0%]
k_{R4}	Vertical compression drag, thrust	[-0.0133%, +57.1%]	[-0.144%, +0%]

Note that in the entries for k_{R4}, vertical compression drag is responsible for the lower (negative) bound on parameter uncertainty; thrust uncertainty is responsible for the upper (positive) bound. Other than k_{R4}, the other parameters only changed in one direction due to the perturbations. Their uncertainties are thus bounded on one side by zero percent: the estimate with unperturbed test conditions.

In the bounded physical range, the uncertainty in μ_{max} and k_{R1} led to modest effects on acceleration: less than 1.5-percent uncertainty in acceleration, even for the nontrivial uncertainties in these parameters. The estimated parameter μ_{max} is for a tire rolling on grass; when used in the simulator, μ_{max} is for a tire rolling on asphalt and is drawn from literature. This observation suggests that in practice any reasonable error between the literature value of μ_{max} and the true value will not cause the simulated takeoff performance to significantly deviate from a real-life scenario.

Finally, despite the very large uncertainty in the estimate for k_{R4}, variations in this parameter were shown to hardly impact the takeoff roll dynamics. This confirms that the quartic term in Eq. (4) is small in the takeoff operating regime; thus, making the modeled dynamics rather insensitive to estimation errors in k_{R4}.

IV. Turning Characteristics

Several batch simulation studies using the LaRC simulator were conducted to gain insight into the predicted ground handling behavior of the X-57 Mod II across a range of operating conditions. These studies featured open-loop steering commands and recorded high-level vehicle responses such as roll angle, turning radius, and weight on wheels.

A. Roll Angle and Turn Radius Simulation Methodology

To identify an envelope of allowable steering inputs as a function of airspeed, airplane configuration, and wind velocity, the LaRC desktop simulation was used to characterize the behavior of the X-57 model on the ground under a wide variety of operating conditions. Simulations were run across a range of these variables: steady-state airspeeds ranging from 10 to 90 kn (well past the rotation speed of 66 kn) in 10-kn increments, crosswind speeds of 5, 10, and 15 kn, crosswind angles all around the airplane at 15-degree intervals, flap deflections of 0- and 20-degree (takeoff configuration), and 40-degree (landing configuration), and open-loop NWS angles (5-degree increments between the limits of ±20 degrees). To determine the ground handling performance, the turning radius as a result of each open-loop NWS angle command, the roll angle, and the weight on each of the three wheels were captured in each simulation run.

In each simulation run, the airplane model was first given a thrust command and allowed to accelerate and reach the desired steady-state forward ground speed with no NWS angle command. Next, simultaneously the NWS angle being tested was commanded open loop, and the wind was introduced at the appropriate velocity and cross track angle. The wind cross track angle was defined as the heading of the wind with respect to the heading of the airplane model at the beginning of the turn. In each simulation, the elevator and ailerons were held at zero deflection. The rudder, meanwhile, deflected proportionally between its limits of ±26 degrees with regards to the NWS command. The simulated airplane position history $x(t)$ and $y(t)$ in response to the NWS command was then used to estimate the radius of curvature of the turn; the turn radius R, given by Eq. (7).

$$R = \frac{\left[1 + \left(y'(x)\right)^2\right]^{\frac{3}{2}}}{|y''(x)|} \tag{7}$$

The turn radius generally decreased over a short transient period after the NWS turn was commanded before reaching a single steady-state value that was recorded for the simulation. In addition to turning, in each simulation the airplane model experienced rolling about the longitudinal axis when the NWS was commanded. Again, this included some transient effects before settling to a steady-state roll angle that was recorded for each simulation. Along these lines, the weight-on-wheels parameters were also recorded for each case to observe if the roll angle became so severe as to cause a wheel to actually lift from the ground.

B. Straight-line Steering Angle Search Methodology

The first desktop simulation study returned data on turning radius as a function of open-loop NWS input. Additional work searched the NWS command space to precisely identify the NWS input required to maintain a straight-line path on the ground. Effectively, this is the NWS input required to achieve an infinite turning radius and provides intuition regarding any potential control saturation on the takeoff roll. Simulations were run across the same ranges of steady-state ground speeds, crosswind speeds, crosswind angles, and flap deflections as before. To identify the appropriate steering angles, the problem was framed as an optimization problem, seeking the steering angle that minimized the curvature of the airplane path. A modified Fibonacci search algorithm was applied to perform this minimization.

To achieve the finest resolution for a given number of function evaluations, the Fibonacci search algorithm prescribes the locations in a bounded single-variable design space to sample an objective function at each optimization iteration. In the first iteration, two objective function evaluations are executed for different design variable values. The new bounds for the design space are presumed to be the region that excludes the design point with the higher objective function value. In each ensuing iteration, one additional objective function evaluation is completed, and the bounds are once again shrunk to exclude the highest objective function value. The ratio between the size of the design

space after consecutive iterations is the ratio between the nth and $(n-1)$th member of the Fibonacci sequence, where n is the number of iterations remaining.

A pitfall of the Fibonacci search algorithm is that it provides no guarantee of global optimality. In the steering angle search problem, the solver often erroneously cropped out the portion of the design space containing the correct minimizer early in the iteration cycle. Since most of the minima were relatively small angles close to zero, the solver had a tendency to select regions with the wrong sign in the first step, which led to poor performance. Possible risk factors for this behavior include steep gradients, inflection points, and local minima in the objective function, as well as minimizers near the initial interrogations of the design space. To counter this premature and incorrect convergence, a "drifting Fibonacci search" algorithm was implemented instead.

At each iteration, the design space is cropped to a region including the prescription from the standard Fibonacci search plus an additional space; this additional space is selected by observing the gradient of the objective, based on the bounds of the Fibonacci prescription. The additional space is added in the direction that the gradient is decreasing, with a width being a fraction of the width of the current region. The fractional constant β is a hyperparameter to be tuned by the engineer and should be less than one to ensure that the search area is actually decreasing at each iteration. In this manner, the Fibonacci search area is allowed to "drift" down the objective function gradient while still converging on the optimum. The search area does not provide a guarantee of global optimality and slows down the convergence process (slower for larger values of β); however, many of the favorable convergence characteristics of the Fibonacci search are combined with the ability to adapt to the objective topology function to better identify the optimum. Applied to the steering angle search problem, the drifting Fibonacci search algorithm provided superior performance at locating the global optimum for several validation test cases when compared to the standard Fibonacci search algorithm.

C. Turning Characteristics Results Summary

The turning and rolling characteristics were thereby characterized across the range of NWS angles, airplane speeds, wind speeds, wind cross track angles, and flap configurations. By fixing three of these variables, this data could be visualized two dimensions at a time to help develop an idea for the ground handling operating envelope. Figure 5 illustrates the roll angle experienced by the X-57 model across a range of NWS angles and airspeeds experiencing a 15-kn quartering tailwind from the right. The quartering tailwind represents the worst-case scenario for roll tendencies at high speed. Figure 5a illustrates the rolling tendencies of the simulated airplane in the takeoff configuration (rotation speed 66-kn IAS [2]); Fig. 5b illustrates the tendencies in the landing configuration (landing speed 75-kn IAS [2]).

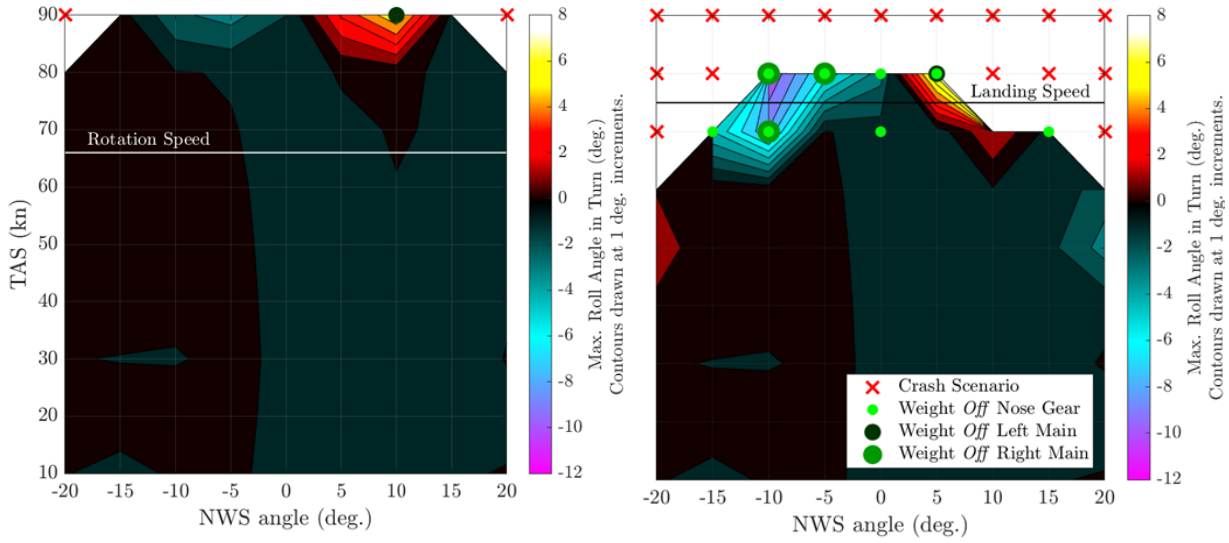

a) Takeoff configuration (20-degrees of flaps). **b) Landing configuration (40-degrees of flaps).**

Fig. 5 Roll angles experienced by the X-57 Mod II model across the ground handling envelope, for a 15-kn quartering tailwind from the right.

Significantly different behavior is observed above the rotation speed. In the takeoff configuration at 90 kn, a 10-degree left nosewheel deflection can be seen, the skid is severe enough to lift the left main landing gear off the ground. Moreover, if full nosewheel deflection is commanded in either direction at this speed, the roll angle in the turn does not actually reach a steady state and diverges into a roll over and crash. More flap extension, as shown in the landing configuration of Fig. 5b, exacerbated the roll and skid tendencies. As a result, the airplane model experienced a wheel or multiple wheels leaving the ground at speeds as low as 70-kn IAS. Additionally, for extreme control inputs, a roll over was also encountered at this speed. At higher speeds, roll and skid behavior was further degraded; at 90-kn IAS the airplane was not controllable on the ground using solely NWS in the landing configuration.

No such tipping behavior, however, was encountered below the rotation speed, where the actual airplane would be on the ground under normal operating circumstances in the takeoff configuration. In the landing configuration, tipping could be avoided by not commanding large inputs at speeds near the landing speed; the weight-off-wheels tendencies would not be a problem because the airplane slows quickly from these speeds during the landing roll. Beyond the worst-case crosswind scenario, illustrated in Fig. 5, there were also no roll upsets in this velocity regime, irrespective of the flap configuration or crosswind nature; thus, the roll angle analysis essentially validated the current rotation and landing speeds, and the Tecnam® crosswind limit of 15 knots.

Lastly, Fig. 6 illustrates the turning radii achieved by the X-57 model across the same range of velocities and NWS angles. The turning radius data were augmented with the straight-line steering data results, which effectively specified the NWS command for each test condition for an "infinite" turning radius.

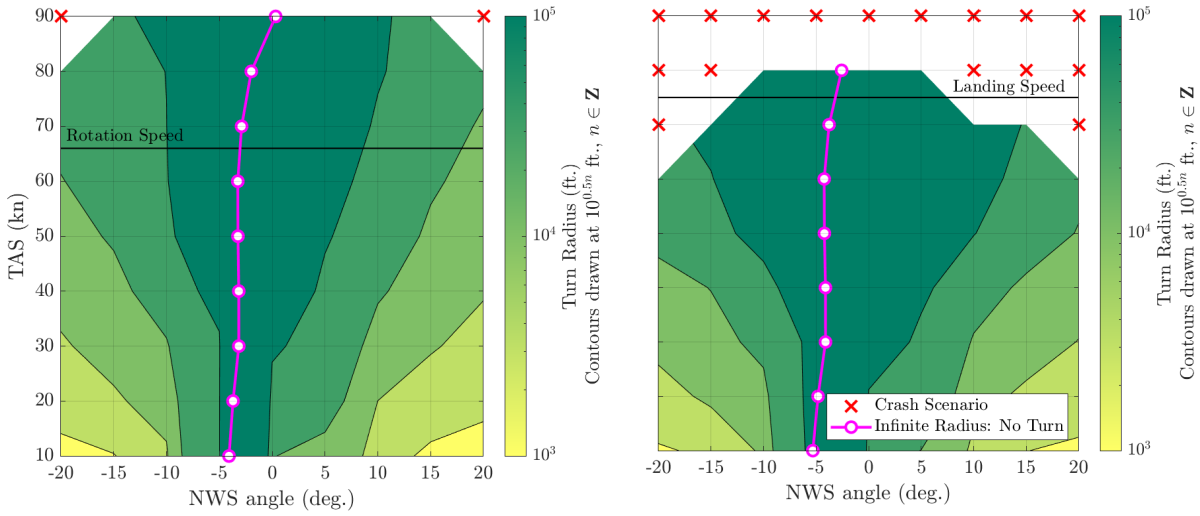

a) Takeoff configuration (20-degrees of flaps). **b) Landing configuration (40-degrees of flaps).**

Fig. 6 Turning radii achieved by the X-57 Mod II model across the ground handling envelope, for a 15-kn quartering tailwind from the right.

Graphics such as Fig. 6 can be used to predict expected turning performance under different ground speeds, configurations, and NWS commands. To connect this analysis with the previous roll angle analysis, Fig. 6 is equipped with the same annotations for the roll upset crashes as Fig. 5. Note: the actual airplane is capable of a tighter turn radius, more persistent weight-on-wheels behavior, and smaller roll angles than those illustrated here by using differential braking and elevator and aileron wind corrections. These capabilities were not quantified at this stage, however; no braking, elevator, or aileron commands were issued in any of these simulations. On the opposite end of the spectrum from tight turn radii, throughout the flight envelope, the straight-line steering command never suggested any problems with control saturation, generally falling below one quarter of the maximum commanded deflection. In the particular configuration and crosswind velocity, shown in Fig. 6, the command is about 4-degree right steering to correct for the quartering tailwind from the right. At higher speeds, this command requirement decreases as the crosswind component becomes a smaller fraction of the forward velocity of the airplane.

V. Piloted Simulator Testing of Ground Handling Qualities

While the desktop simulation was used to quantitatively verify that the predicted X-57 landing gear possessed favorable behavior on the ground, a series of piloted simulator experiments were developed to gather structured feedback from the project pilot on the handling qualities of the airplane.

The piloted simulator, shown in Fig. 7, was developed to mimic the cockpit of the X-57 airplane as closely as possible. The dashboard simulator has a digital representation of the exact type and location of the left and right airplane instrument panels. Also on the dashboard are hardware that identically match the physical switches, flaps lever, and landing gear handle that would be found in similar locations in the X-57 cockpit. In addition, the simulator power and control inceptors replicated the actual placement of the X-57 inceptor, force feel, and travel. Like the airplane, the simulator rudder pedals simultaneously control the rudder deflection and the nose wheel steering. Included on the rudder pedals are toe brakes, which operate individual brakes on the main wheels. A high-definition, out-the-window environment is projected onto a 34- by 120-degree curved screen, which provides realistic views for the pilot.

Fig. 7 The X-57 fixed-base piloted simulator.

The investigation produced both quantitative (ability to operate the airplane simulation within defined margins, and Cooper-Harper [12] ratings) and qualitative (pilot comments) metrics designed to uncover potential pilot-in-the-loop difficulties with the Mod II configuration prior to flight. To evaluate the ground handling qualities, three evaluation tasks were performed in the simulator: Runway Offset Capture and Hold (ROCH), Maximum Heading Capture and Stabilization (MaxHCAS), and Runway Centerline Tracking (RCT) [13].

A. Runway Offset Capture and Hold (ROCH)

1. Experiment Description

In the ROCH maneuver, the pilot is tasked with quickly capturing and tracking parallel reference lines. This task seeks to identify maneuverability limitations and any pilot-induced oscillation (PIO) tendencies of the airplane. Handling qualities are rated as acceptable or not based on position data from the simulator and pilot handling qualities assessments and observations.

The airplane simulation is initially established in a ground roll along the runway centerline at constant speed. The pilot will then turn to capture a parallel runway reference line, spaced about 40-feet (ft) away from the centerline. This reference line is implemented visually in the piloted simulation out-the-window display. The intercept angle should be approximately four to seven degrees, and to aid the pilot, a set of angle cues is provided in the visual display of the simulator. These cues will translate, but not rotate, with the airplane simulation to inform the pilot what a 4- to 7-degree intercept angle to the runway heading looks like at all times. Figure 8 illustrates how these cues should move with the airplane.

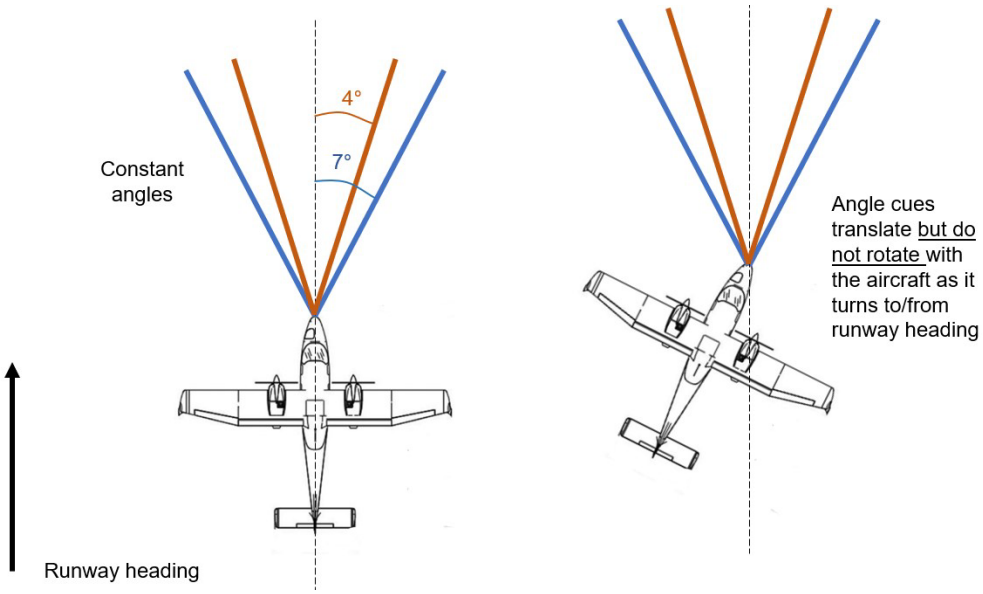

Fig. 8 The ROCH heading cues for the simulation pilot to reference. Note: angles are not to scale.

The pilot should arrive at the reference line and then track that line for five seconds, or for as much time as needed to stabilize the heading. Note that leading the reference line, or turning early to start tracking smoothly, is permissible. Next, the pilot will perform the capture task in reverse: beginning at the reference line, turning to capture the runway centerline, and stabilizing there. The task will be repeated by moving down the runway as many times as needed until the pilot is ready to rate the handling qualities of the configuration in this task.

The series of captures was repeated at velocities of 40, 50, 60, and 70 kn, and for all flap configurations: 0, 20, and 40 degrees. The handling performance was judged on the ability to achieve certain overshoot (within 2-ft desired, within 5-ft adequate) and tracking (within 2-ft desired, within 5-ft adequate) tolerances.

2. Experiment Results

Figure 9 illustrates the results of the ROCH experiments. Separate Cooper-Harper ratings were assigned for the two phases of each maneuver: 1) the gross-tracking initial capture of the new reference; and 2) fine tracking after the initial capture. Additionally, indicators are presented that show whether the quantitative overshoot and tracking tolerances were met. The markers over the initial capture handling quality ratings correspond to the overshoot tolerance, and markers over the fine tracking ratings correspond to the tracking tolerance.

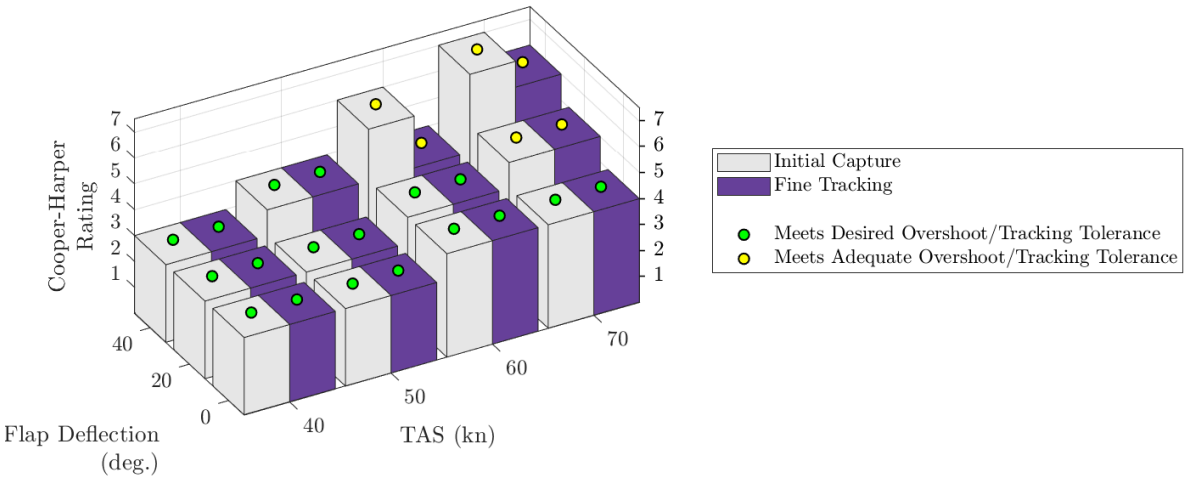

Fig. 9 Cooper-Harper handling qualities ratings for the ROCH evaluation.

Favorable handling qualities were generally observed below the nominal rotation speed of 66 kn, with the evaluation pilot noting that greater workload was required at higher speeds in the landing configuration (full 40-degree flaps). Approaching and surpassing the rotation speed in the clean configuration, the pilot felt that progressively more lead was demanded for both gross and fine tracking, though in general this lead was not found to be problematic, and the desired overshoot and tracking specifications were consistently met. Beginning at 60 kn in the takeoff configuration of 20-degree flaps, the pilot observed skidding (as predicted by the batch simulation work discussed in Section IV). In addition to significant skidding, significant roll was also encountered in the landing configuration beginning at 60 kn during the gross acquisition phase. Figure 10 gives examples of ground tracks for the three configurations at 60 kn and illustrates the impact of this skidding behavior on capture and tracking performance. For clarity, the time history begins when the airplane simulation is 10-ft away from the reference line.

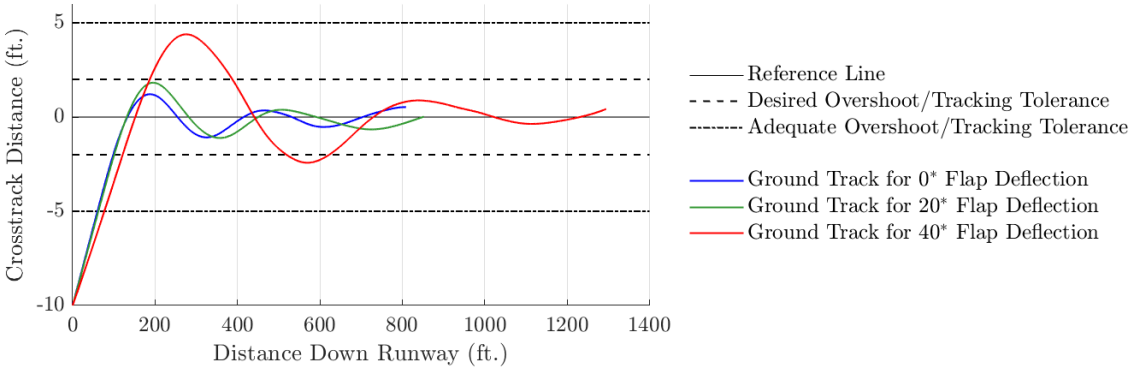

Fig. 10 Examples of ground track plots at 60 kn in the ROCH evaluation. Note: axes not to scale.

For the takeoff configuration, progressively larger amounts of skidding at higher velocities correlated with a progressively degraded handling quality rating and an inability to attain the desired tolerances, though the adequate overshoot and tracking tolerances were still met. At 70 kn in the landing configuration, rolling tendencies were noted in both fine and gross tracking; PIOs were also encountered during the initial capture, as shown in Fig. 11.

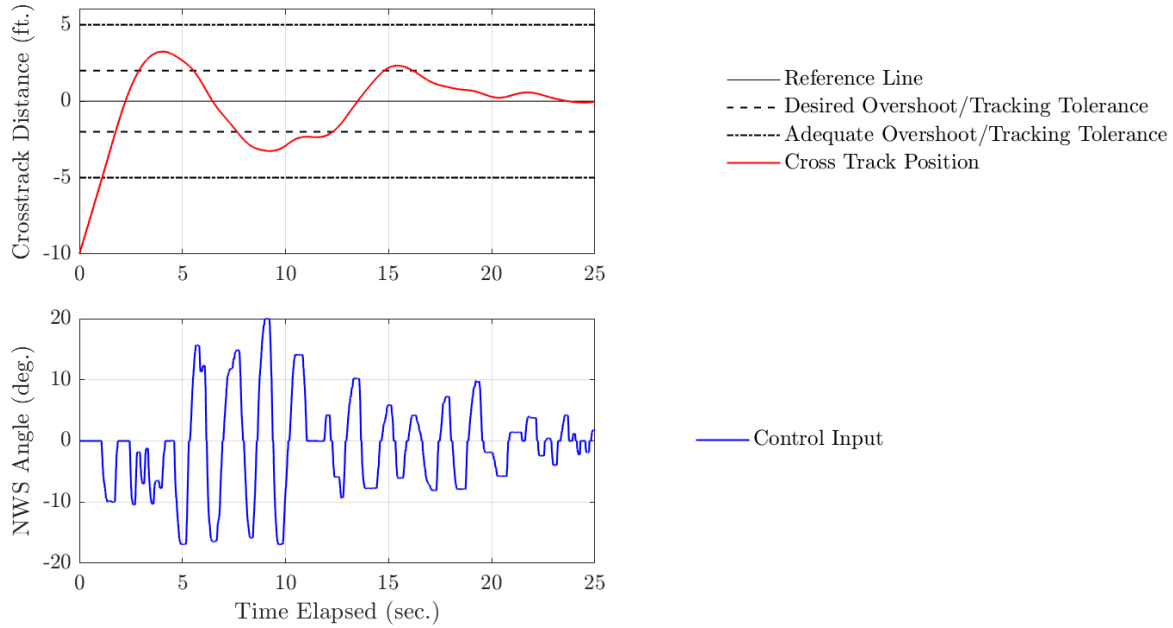

Fig. 11 Cross track and steering input for a ROCH maneuver in the landing configuration at 70 knots.

The PIO can be observed between about 5 seconds and 12 seconds in Fig. 11, where large steering angles are commanded in a labored effort to acquire the reference line. The evaluation pilot commented that free play in the steering controls contributed to the PIO. Generally, the NWS angle deflects proportionally with respect to the pilot-commanded rudder pedal deflection. For small, rapid rudder pedal deflections, however, the NWS angle is not as responsive because of slack in the control cables. This effective low gain in the control system induces higher pilot gain to compensate, inducing the PIO. Despite these factors leading to markedly degraded handling qualities ratings, the airplane simulation was still controllable and attained the adequate overshoot and tracking tolerances even under these conditions.

In practice though, the airplane will decelerate through the landing speed and would not be subjected to maneuvering at speeds around 70 kn for too long. Other than these occurrences impacting handling qualities at high speeds, the ROCH evaluation series confirmed adequate handling qualities below the rotation speed in the takeoff configuration and below the landing speed in the landing configuration.

B. Maximum Heading Capture and Stabilization (MaxHCAS)

1. Experiment Description

Maximum Heading Capture and Stabilization (MaxHCAS) is similar to ROCH and involves the acquisition and tracking of a parallel reference line; it differs, however, in that pilot steering inputs to intercept the reference are specified rather than the approximate intercept angle. This task seeks to evaluate the handling response of the system with regards to varying levels of aggressiveness, identify maneuverability limitations as functions of aggressiveness, and uncover any PIO tendencies.

The airplane simulation is established in a ground roll along the runway centerline at constant speed. The pilot will turn to capture a parallel runway reference line, spaced about 40-ft away from the centerline. To evaluate different levels of command aggressiveness, the initial rudder input towards the reference line should be open loop, either a "nominal" (approximately half-deflection) or a "maximum" (full deflection) rudder input. This deflection will be applied for a step-pulse of approximately one second.

Upon crossing the reference line, the pilot should immediately capture that line and stabilize. By contrast to ROCH, leading the line by turning early is not permitted. The line should then be tracked for five seconds, or for as much time as needed to stabilize the heading. The task will be continued moving down the runway as many times as needed until the pilot is ready to rate the handling qualities of the configuration in this task.

The series of captures was repeated at velocities of 40, 50, 60, and 70 kn in the takeoff flap configuration. The handling performance was judged on the ability to achieve certain initial overshoot (within 5-ft desired, within 15-ft adequate; and tracking tolerances (within 2-ft desired, within 5-ft adequate). Note that the overshoot tolerances are looser than those for ROCH since leading the reference is not allowed in MaxHCAS.

2. Experiment Results

Figure 12 illustrates the results of the MaxHCAS experiments. Figure 12a shows Cooper-Harper ratings for the nominal input, and Fig. 12b shows those for the full-deflection input. Separate Cooper-Harper ratings were assigned for the two phases of each maneuver: 1) the gross-tracking initial capture of the new reference; and 2) fine tracking after the initial capture. Additionally, indicators are presented that show whether the quantitative overshoot and tracking tolerances were met. The markers over the initial capture handling quality ratings correspond to the overshoot tolerance, and those over the fine tracking ratings correspond to the tracking tolerance.

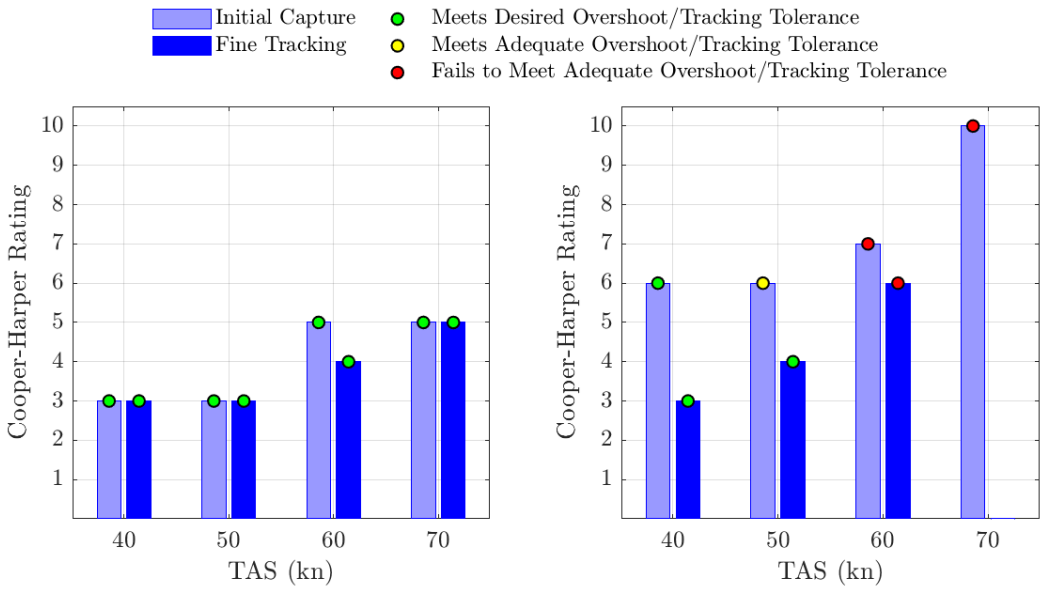

a) Nominal-deflection initial input. **b) Maximum-deflection initial input.**

Fig. 12 Cooper-Harper handling qualities ratings for the MaxHCAS evaluation.

Throughout the experiment, settling the airplane simulation into the fine tracking task after the initial input received better ratings than the initial capture as there was no requirement for aggressiveness during the latter phase. Throughout the range of speeds tested, both the nominal-input initial capture and the ensuing fine tracking tasks received satisfactory ratings and achieved the desired tolerances. Approaching and beyond the rotation speed, the evaluation pilot noted the onset of skidding resulting in mild to moderate handling qualities deficiencies, though the desired performance was still met. Skidding noted throughout these maneuvers was consistent with the analysis performed in Section IV.

An aggressive initial input led to more objectionable dynamic behavior during the initial capture; at speeds approaching and surpassing the rotation speed, aggressive control inputs raised serious handling qualities concerns. While all tasks were at least able to be completed below the rotation speed, the desired overshoot tolerance was not reached at or above 50 kn, and even the adequate overshoot performance was not achieved at or above 60 knots. Fine tracking handling qualities were slightly more favorable, meeting the desired tracking tolerance up to 50 kn and the adequate tolerance up to 60 knots. At 60-kn ground speed, the pilot observed skidding in the aggressive initial capture, making it difficult to settle the simulation into fine tracking; at 70 kn the maximum-deflection initial capture attempt resulted in a loss of control and the inability to begin fine tracking at all. Figure 13 shows examples of ground tracks for both the nominal and aggressive inputs at 60 kn - the highest speed that did not encounter loss of control. For clarity, the time history begins when the airplane is 20-ft away from the reference line.

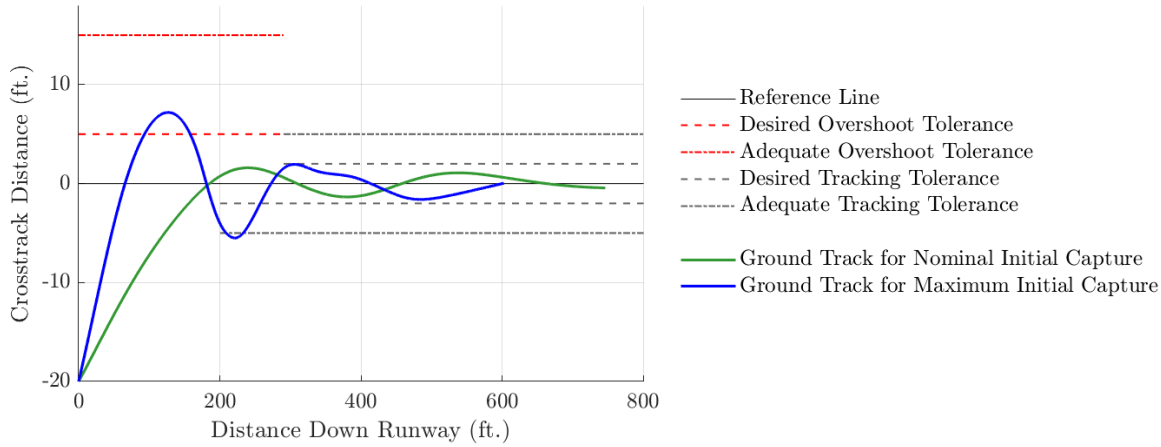

Fig. 13 Examples of ground track plots at 60 kn in the MaxHCAS evaluation. Note: axes not to scale.

Whereas the desired overshoot and tracking criteria are met for the nominal initial input, the aggressive initial input causes a much slower recovery and transition to fine tracking. Consequently, the test with an aggressive initial capture fails to meet even the adequate overshoot and tracking tolerances. Figure 14 further illustrates the scenario, portraying the commanded NWS angle time histories for the same full-deflection and half-deflection initial captures at 60 kn, just below the rotation speed. Note that the horizontal axis of Fig. 14 begins before the initial turn to intercept the new reference and does not synchronize with the horizontal axis of Fig. 13.

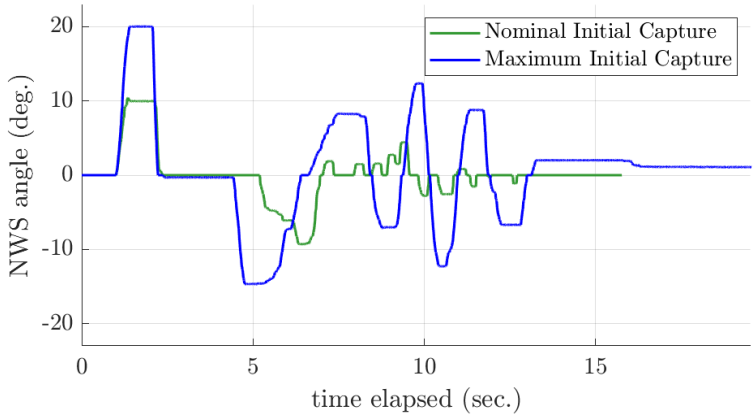

Fig. 14 Comparison of MaxHCAS nosewheel steering (NWS) angle time histories at 60-kn ground speed.

Although the pilot is not required by the experiment to be aggressive during fine tracking after an aggressive initial input, the aggressive initial capture demands similarly control-intensive commands to transition from gross to fine tracking. The result is significantly higher control efforts in fine tracking than are seen in the nominal initial capture case, leading to the failed specifications and degraded handling quality rating. The evaluation pilot noted that at higher speeds, the aggressive initial capture using maximum NWS was unnatural and would in practice be better accomplished using differential braking.

The results suggest that for ground velocities below the rotation speed, the piloted simulation exhibits satisfactory handling qualities for normal steering inputs. Aggressive maneuvering can be tolerated at lower speeds but should be avoided at speeds approaching the rotation speed to avoid degraded handling qualities or potential loss of control.

C. Runway Centerline Tracking (RCT)

1. Experiment Description

In the RCT maneuver, the pilot is tasked with continuously and aggressively tracking the runway centerline in the presence of disturbances such as simulated crosswind gusts. This task seeks to evaluate the closed-loop handling response, pilot-vehicle system sensitivity to disturbances, and any PIO tendencies.

The airplane simulation is established in a ground roll along the runway centerline at constant speed. A sum-of-sines disturbance is applied to the NWS command, approximately simulating the effect of a variable crosswind on the airplane. This sum-of-sines disturbance also has a constant bias to simulate a steady crosswind in addition to the gusts. No component of the sum-of-sines has a frequency higher than 3 Hz, and at no point does the magnitude of the summed signal exceed five degrees of NWS steering. The 5-degree limit comes from the analysis in Section IV showing that given the crosswind limitation of the X-57 airplane, no more than five degrees of NWS should ever be required to reject a crosswind and steer in a straight line. Five degrees of NWS should thus represent the maximum disturbance caused by a crosswind. Finally, the amplitudes of each of the sum-of-sines components ramp up over time before reaching final values to assess the handling characteristics of the airplane simulation under different intensities of disturbances. Under the influence of this disturbance, the pilot is to continue tracking the runway centerline as closely and aggressively as possible.

The series of captures was repeated at velocities of 40, 50, 60, and 70 kn, and for all flap configurations: 0, 20, and 40 degrees. In each test, tracking was continued moving down the runway until the pilot was ready to rate the handling qualities of the configuration being tested. The handling performance was judged on the achieved tracking tolerances (within 2-ft desired, within 5-ft adequate).

2. Experiment Results

Figure 15 illustrates the results of the RCT experiments. The Cooper-Harper ratings for this series of tasks are illustrated with vertical bars, color-coded for the different flap configurations. Additionally, indicators are presented that show whether the quantitative tracking tolerances were met.

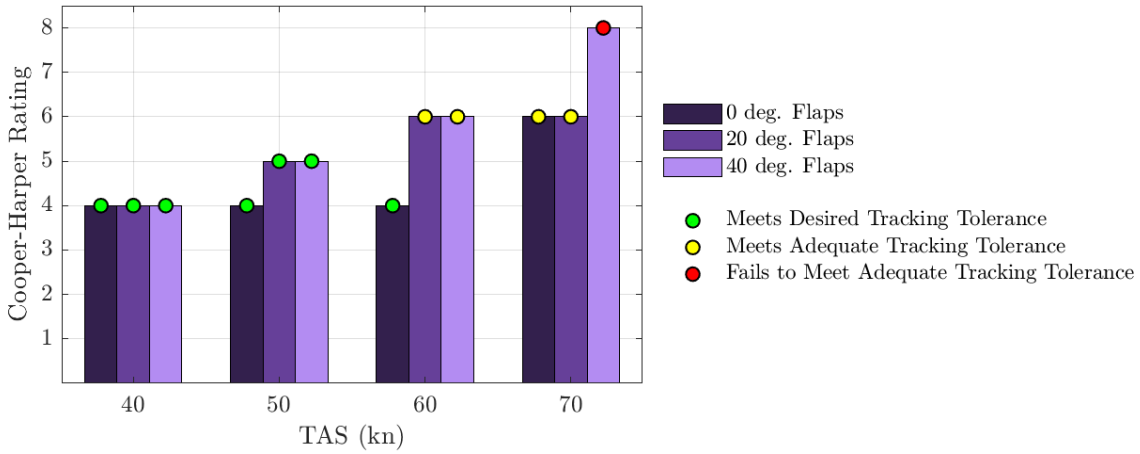

Fig. 15 Cooper-Harper handling qualities ratings for the RCT evaluation.

In the clean configuration, some skidding was encountered at speeds at and above 50 kn, although only noticeable problems occurred with tracking at 70 knots. Lowering 20-degree of flaps increased the magnitude of pilot inputs required to closely track the reference and exacerbated the skidding behavior. Tracking performance was thus slightly inferior to the clean configuration with the desired tolerance met at 50 kn and below, and the adequate specification met at 60 knots and above. Finally, the full-flap configuration experienced similar skidding trends and required even larger control inputs to continue tracking the reference. Moreover, at 70 kn the airplane had a tendency to take off on its own; there was virtually no control authority due to this behavior, and the tracking behavior fell outside of the acceptable range. Figure 16 illustrates ground tracks for the landing configuration across the four velocities examined.

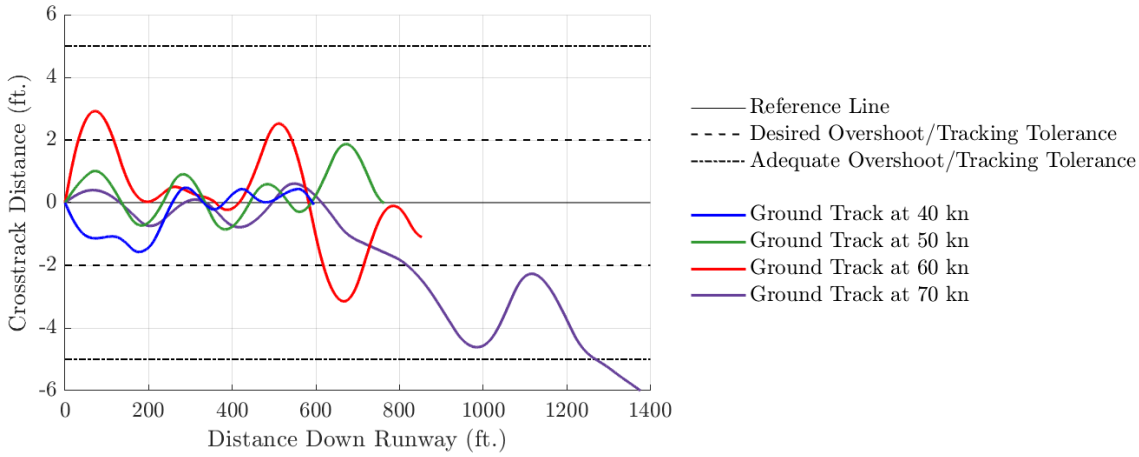

Fig. 16 Examples of ground track plots in the RCT evaluation with 40-degree flaps. Note: axes not to scale.

At higher speeds, the airplane simulation offered progressively less control authority and the pilot was only able to control it to progressively looser tolerances. Note that the four ground tracks were produced in response to different sinusoidal disturbances. In practice, the airplane will decelerate through the landing speed and would not be subjected to maneuvering at speeds around 70 kn for prolonged time periods.

In all, the RCT evaluations demonstrated that even in the face of disturbances equivalent to gusts of the maximum allowed crosswind, with effort the pilot could track the airplane simulation along a straight reference path through the normal operating envelope.

VI. Conclusion

The ground dynamics model of the X-57 airplane was refined by developing and fitting a detailed model of the tire rolling drag using manufacturer data from Tecnam®. Uncertainty in the acceleration dynamics was bounded as a function of uncertainty in the test conditions for the manufacturer data, showing that the kinematics of the airplane are insensitive to modeling errors but are noticeably different compared to those predicted with the old rolling drag model. The X-57 desktop simulation was equipped with this new landing gear model that was used to thoroughly sweep across operating conditions to analyze the landing gear model and predict the ground maneuvering capabilities of the X-57 Mod II. Roll angle and turning radius were analyzed as functions of ground speed, flap configuration, and crosswind velocity. The model predicted that within the ground operating envelope, roll upsets would not occur for almost any open-loop steering command, and the NWS would command sufficient authority to maintain a straight ground track in the presence of a steady-state crosswind. The model also predicted potential control difficulties for maximum-deflection steering inputs at speeds near and above the landing speed that pilots should avoid in practice. This batch simulation analysis thus validated the Tecnam® ground operating envelope under open-loop control inputs.

A piloted simulation investigation was then conducted to verify pilot-in-the-loop characteristics and identify potential difficulties with handling qualities. Runway Offset Capture and Hold (ROCH) evaluations suggested that there exist no maneuverability limitations or pilot-induced oscillation (PIO) tendencies below the rotation speed in the takeoff configuration. The results also identified modes of degraded handling characteristics resulting from skidding and rolling at high speeds in the landing configuration, though in practice the airplane will decelerate quickly from these speeds. Maximum heading capture (MHC) and hold task results suggest that below the rotation speed the simulation exhibits satisfactory handling qualities for moderate steering inputs in the takeoff configuration. The airplane model responds less favorably for unusually aggressive steering commands at these speeds; such inputs should be avoided near the rotation speed. Beyond the rotation speed, such aggressive steering commands could even lead to loss of control. Finally, runway centerline tracking (RCT) evaluations demonstrated that even in the face of disturbances equivalent to gusts of the maximum allowed crosswind, the pilot could track the airplane simulation along a straight reference path for all conditions below the rotation speed in the takeoff configuration. The closed-loop ground handling qualities were generally as desired and still adequate at higher speeds where increased skidding and lower control authority were noted. Critical closed-loop sensitivities to disturbances were only noted in the landing configuration at high speeds that, again, the airplane will not experience for long in practice. In all, the piloted simulation evaluation validated the Tecnam® ground operating envelope under closed loop, piloted control.

Although ground handling and taxiing will not be a focus in the upcoming X-57 Mod II flight-test campaign, data gathered may be applied using the methods in this paper to further refine the dynamics of the airplane model. In the meantime, the techniques and results shown here provide an improved image of the characteristics of the airplane, progressively gearing up to demonstrate the fruits of distributed electric propulsion.

Acknowledgments

The authors thank David E. Cox, James R. Reynolds, and J. Dana McMinn for their review of the rolling drag analysis, and Timothy L. Williams for his work in and review of the piloted ground handling qualities evaluation.

References

[1] Borer, N. K., Patterson, M. D., Viken, J. K., Moore, M. D., Clarke, S., Redifer, M. E., Christie, R. J., Stoll, A. M., Dubois, A., Bevirt, J., Gibson, A. R., Foster, T. J., Osterkamp, P. G., "Design and Performance of the NASA SCEPTOR Distributed Electric Propulsion Flight Demonstrator," AIAA Paper 2016-3920, June 2016. doi.org/10.2514/6.2016-3920

[2] Construzione Aeronautiche Tecnam, *P2006T Aircraft Flight Manual*, Doc. No. 2006/044, 4th ed., Rev. 2, Capua, Italy, March 2017.

[3] Pacejka, H., Bakker, E., and Nyborg, L., "Tyre Modelling for Use in Vehicle Dynamics Studies", SAE Paper 870421, Feb. 1987. doi.org/10.4271/870421

[4] van Es, G. W. H., "Method for Predicting the Rolling Resistance of Aircraft Tires in Dry Snow," *Journal of Aircraft*, Vol. 36, No. 5, 1999, pp. 762-768. doi.org/10.2514/2.2531

[5] Pytka, J. A., "Identification of Rolling Resistance Coefficients for Aircraft Tires on Unsurfaced Airfields," *Journal of Aircraft*, Vol. 51, No. 2, 2014, pp. 353-360. doi.org/10.2514/1.C031088

[6] Lindström, M., "Aircraft Rolling Resistance in Loose Dry Snow," National Road & Traffic Institute (VTI), Report 173A, Fack, Sweden, 1979.

[7] Constantini, E. A. C., Urbano, F., and L'Abate, G., "Soil Regions of Italy," Italian National Council for Agricultural Research.

[8] Krishna, Bala, "Minimum Depth of Foundation," *Civil Planets*, retrieved 24 Jun 2020, https://civilplanets.com/minimum-depth-of-foundation/ [retrieved 15 April 2022].

[9] "Dirt and Mud – Densities," *The Engineering Toolbox, (2010)*, https://www.engineeringtoolbox.com/dirt-mud-densities-d_1727.html [retrieved 15 April 2022].

[10] Hooke, R. and Jeeves, T. A., "'Direct Search' Solution of Numerical and Statistical Problems," *Journal of the ACM*, Vol. 8, No. 2, 1961, pp. 212-229. doi.org/10.1145/321062.321069

[11] "Friction - Friction Coefficients and Calculator," *The Engineering Toolbox*, 2004, retrieved 25 Jun 2020, URL: https://www.engineeringtoolbox.com/friction-coefficients-d_778.html [retrieved 15 April 2022].

[12] Harper. R. P. and Cooper, G. E., "Handling Qualities and Pilot Evaluation," *Journal of Guidance*, Vol. 9, No. 5, 1986, pp. 515-529. doi.org/10.2514/3.20142

[13] Klyde, D. H., Magdaleno, R. E., Myers, T. T., and Reinsberg, J. G., "Development and Evaluation of Aircraft Ground Handling Maneuvers and Metrics," AIAA Paper 2001-4011, Aug. 2001. doi.org/10.2514/6.2001-4011